Original Theory of NGD Low Pass-High Pass Composite Function for Designing Inductorless BP NGD Lumped Circuit

Blaise Elysée Guy Ravelo, Samuel Ngoho Moungoho, Glauco Fontgalland, Lala Rajaoarisoa, Wenceslas Rahajandraibe, Rémy Vauche, Zhifei Xu, Fayu Wan, Junxiang Ge, Sébastien Lallechere

IEEE Access
Multidisciplinary ⋮ Rapid Review ⋮ Open Access Journal

Received October 12, 2020, accepted October 19, 2020, date of publication October 22, 2020, date of current version November 3, 2020.

Digital Object Identifier 10.1109/ACCESS.2020.3033038

Original Theory of NGD Low Pass-High Pass Composite Function for Designing Inductorless BP NGD Lumped Circuit

BLAISE RAVELO[1], (Member, IEEE), SAMUEL NGOHO[2], GLAUCO FONTGALLAND[3], (Senior Member, IEEE), LALA RAJAOARISOA[4], (Member, IEEE), WENCESLAS RAHAJANDRAIBE[5], (Member, IEEE), RÉMY VAUCHÉ[5], (Member, IEEE), ZHIFEI XU[6], (Member, IEEE), FAYU WAN[1], (Member, IEEE), JUNXIANG GE[1], (Associate Member, IEEE), AND SÉBASTIEN LALLÉCHÈRE[7], (Member, IEEE)

[1]School of Electronic and Information Engineering, Nanjing University of Information Science and Technology, Nanjing 210044, China
[2]Association Française de Science des Systèmes (AFSCET), 75017 Paris, France
[3]Applied Electromagnetic and Microwave Laboratory, Federal University of Campina Grande, Campina Grande 58429, Brazil
[4]IMT Lille Douai, Unité de Recherche en Informatique et Automatique, University of Lille, 59000 Lille, France
[5]Aix-Marseille Univ, Univ Toulon, CNRS, IM2NP, 13007 Marseille, France
[6]Electromagnetic Compatibility Laboratory, Missouri University of Science and Technology, Rolla, MO 65401, USA
[7]Institut Pascal, SIGMA Clermont, Université Clermont Auvergne, 63000 Clermont-Ferrand, France

Corresponding author: Zhifei Xu (zxfdc@mst.edu)

This work was supported in part by the NSFC under Grant 61601233 and Grant 61750110535, in part by the NSF of Jiangsu under Grant BK20150918, in part by the Jiangsu Innovation and Enterprise Group Talents Plan 2015 under Grant SRCB201526, and in part by the Priority Academic Program Development (PAPD) of Jiangsu Higher Education Institutions.

ABSTRACT This paper aims to develop an original circuit theory of inductorless NGD topology. The considered passive cell comprised of resistor and capacitor elements without inductor operates as a bandpass (BP) NGD function. The specifications of NGD functions are defined. Generally, the BP NGD fully lumped circuits available in the literature operate with resonant RLC-network. In the introduced research work, a lumped circuit was first time identified to exhibit the BP behavior without the presence of inductive component. The inductorless BP NGD topology is inspired from the combination of low-pass (LP) and high-pass (HP) NGD passive cells. Therefore, an original LP-HP NGD composite topology is obtained. The identified BP NGD topology is constituted only by passive RC-networks. Then, theoretical development of BP NGD analysis is explored. The inductorless circuit theory starts with the identification of BP NGD canonical form. Then, the expressions of NGD value, center frequency and attenuation in function of RC-network parameters are established. The synthesis equations allowing to determine the resistor and capacitor elements are derived. Proofs-of-concept are designed and prototypes are fabricated to verify the effectiveness of the developed LP-HP NGD composite theory. To validate the developed original circuit theory, two prototypes of RC-network based LP-HP NGD composite were designed, fabricated, simulated and tested. The two prototypes were synthesized with respect to two different NGD center frequencies 13.5 MHz and 22 MHz. As expected, the calculated, simulated and measurement results are in very good agreement with NGD value of about some negative nanoseconds. In the future, the characterized inductorless topology enable to overcome the traditional limitations of RLC-network based BP NGD circuits because of inductance self-effect limitation.

INDEX TERMS Bandpass (BP) negative group delay (NGD), low-pass/high-pass (LP-HP) NGD composite, circuit theory, inductorless passive topology.

I. INTRODUCTION

The natural or artificial unintentional noise and group delay (GD) effects [1], [2] are one of the most critical phenomena that degrade the performance of electronic circuits. Different alternative technical solutions were explored to overcome this undesirable effect. Topologies and design methods of various filters were explored to minimize this effect.

In brief, the filter functions are found at different stages of electronic systems and they constitute the most familiar

The associate editor coordinating the review of this manuscript and approving it for publication was Liu Hongchen.

electronic functions [3], [4]. In filter theory, we can find three basic filter categories: low-pass (LP), high-pass (HP), and bandpass (BP) behaviors [3], [4]. To increase the communication system performances, new generations of filters based on zeroth order resonance (ZOR) metamaterials have been introduced [5]–[7]. These metamaterial-based filters [5]–[7] are designed, under particular concept, combining left- and right-handed cells.

In parallel with the filter design revolution, it was reported that certain metamaterials are capable to operate with negative refractive index (NRI) [8], [9]. Such metamaterial structures generate naturally the negative group delay (NGD) effect which is analytically linked to the NRI [8], [9]. The existence of the NGD effect was firstly experimented with optical NRI structures [10], [11]. The repeatability of the NGD experimentation was approved with pulse signal propagation through NRI media [10]–[12]. Due to its counterintuitive effect, the NGD effect was a breakthrough for physicists but also for the electronic design engineers. The NGD effect was theoretically and experimentally investigated with active lumped circuits in [12]. It was emphasized that the NGD effect does not contradict the causality principle [13].

To alleviate the issues related to the signal delay [2], [14], equalization techniques using NGD circuits were introduced [15]–[18]. Behind this NGD tentative application, the NGD circuits were implemented differently. For example, in [10], [11], the NGD circuits were used to design stopband and GD equalized BP filters. Other RF and microwave applications were proposed as compensation of oscillators, filters, and communication systems [19]. The NGD circuits were also integrated in the phased array antenna system [20] and to design non-Foster elements [21], [22]. Despite these initiative applications, further research work for understanding and interpretation of the NGD function is necessary. It was emphasized that the NGD function can be generated with various aspects as the NRI metamaterials [10], [11], interference technique [23], [24], active resonator-based distributed circuits [25], microwave transversal filter approach [26], and microstrip circuits [27]–[30]. Mostly research work on the NGD circuit design in last decade was essentially focused on the low-loss and compact passive circuits [8], [9], [20]–[24], [27]–[30]. However, the interpretation of the NGD effect in microstrip circuits raises curious questions for electronic design engineer's non-specialist of NGD function.

A fundamental and academic approach to answer to this curiosity was the initiation of analogy between the filter and NGD behavior [31]–[33]. Based on this similitude behavior, the concept of LP [32] and HP [33] NGD functions was introduced and verified with linear lumped circuits. The filter-NGD analogy opens an unfamiliar way to analyze and design innovative NGD circuits. It can analytically be identified by transfer function (TF) and topological analysis that the fundamental classification of this RF and microwave NGD circuits, available in the literature, belongs to the BP NGD category [17]–[30]. It can also be remarked that these diverse BP NGD circuits [17]–[30] operate, generally, with use of resonant RLC-networks. The theoretical approaches proposed in the most of NGD theory state that NGD center frequencies are equal to the resonance frequency. We demonstrate in the present paper, thanks to the similarity between the filter and NGD behavior, that this statement is not always the case for some particular inductorless topologies. Untypical NGD topologies constituted only by resistor and capacitor lumped components will be originally explored in this paper.

The paper is mainly organized in four different sections described as follows:

- Section II presents the generality on the unfamiliar NGD function. The general approach is based on the consideration of two port system GD expression. Then, based on the graphic representation, the specifications of LP, HP and BP functions are defined.
- Section III focuses on the original circuit theory of inductorless BP NGD topology. The LP and HP composite circuit to synthesize a BP NGD function will be specified. The LP, HP and BP NGD topologies are based on only resistor and capacitor components or RC-networks without self-inductance.
- Section IV elaborates the BP NGD analysis and synthesis. The BP NGD canonical form will be expressed from the LP-HP NGD composite voltage transfer function (VTF) analysis. The synthesis design equation of inductorless circuit in function of the BP NGD specifications will be formulated.
- Section V is dedicated to the discussion on the inductorless BP NGD circuit validation results. The developed BP NGD analysis is limited to the VTF approach. The present study does not take into account the reflection effect as investigated in [34]. Comparison between calculation, simulation, and measurement by designing proofs of concept (PoC) and also fabricating two circuit prototypes in hybrid technology will be discussed.
- Section VI is reserved to the conclusion of the paper.

II. PRELIMINARY DESCRIPTION OF NGD FUNCTION SPECIFICATIONS

This section describes the general representation of the topology as a two-port system. The GD expression is derived from the VTF associated to the system. Then, the concept of LP-HP NGD composite topology is defined. The topology will be elaborated for the inductorless BP NGD circuit theory.

A. ANALYTICAL GENERAL INTRODUCTION

Our topological approach is fundamentally developed by means of circuit and system theory. Accordingly, we consider the black box representation of the two-port system introduced in Fig. 1. The input and output voltages are denoted U_1 and U_2 and the access currents by I_1 and I_2, respectively.

The analytical representation is given by the generalized Ohm's law:

$$\begin{bmatrix} U_1(s) \\ U_2(s) \end{bmatrix} = [Z(s)] \times \begin{bmatrix} I_1(s) \\ I_2(s) \end{bmatrix}. \quad (1)$$

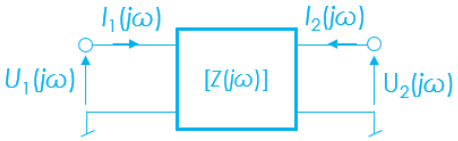

FIGURE 1. Two-port black box system represented by its impedance matrix.

where $s = j\omega$ is the Laplace variable by denoting the angular frequency, ω. The associated Z-matrix is analytically represented by:

$$[Z(s)] = \begin{bmatrix} Z_{11}(s) & Z_{21}(s) \\ Z_{21}(s) & Z_{11}(s) \end{bmatrix}. \tag{2}$$

The VTF derived from this Z-matrix is given by:

$$T(s) = \left.\frac{U_2(s)}{U_1(s)}\right|_{I_2=0}. \tag{3}$$

By taking into account definition (1), this VTF can be rewritten as:

$$T(s) = \frac{Z_{21}(s)}{Z_{11}(s)}. \tag{4}$$

So far, the NGD functions are not simply familiar to the non-specialist electronic engineers. To increase the non-specialist familiarity, we propose the basic specifications of LP, HP and BP NGD functions. The preliminary definitions of NGD function specifications will be described in the following paragraphs.

B. RECALL ON THE FREQUENCY DOMAIN PARAMETERS

The analysis of the VTF should be performed in the frequency domain. The main approach of the frequency domain analysis depends on the magnitude and phase basically defined by:

$$T(\omega) = \left|\frac{Z_{21}(j\omega)}{Z_{11}(j\omega)}\right| \tag{5}$$

$$\varphi(\omega) = \arg\left[Z_{21}(j\omega)\right] - \arg\left[Z_{11}(j\omega)\right]. \tag{6}$$

The frequency dependent GD response is defined by:

$$GD(\omega) = -\frac{\partial\varphi(\omega)}{\partial\omega}. \tag{7}$$

This system is an NGD function if we can find an angular frequency, $\omega_x > 0$, where

$$GD(\omega_x) < 0. \tag{8}$$

The NGD cut-off frequencies are the roots of equation:

$$GD(\omega) = 0. \tag{9}$$

The generalization of this analytical approach for NGD functions can be done by analogy with the filters.

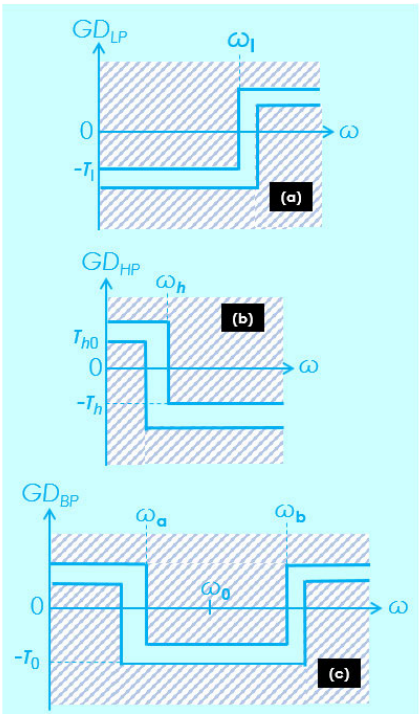

FIGURE 2. (a) LP, (b) HP, and (c) BP NGD ideal responses.

C. LP, HP, AND BP NGD FUNCTION SPECIFICATION INTRODUCTION

The ideal responses of the LP, HP, and BP NGD functions are represented in Fig. 2(a), Fig. 2(b), and Fig. 2(c), respectively.

As initial step of the circuit design, the desired specifications must be chosen. For example, in the present paper, the main desired specifications are defined by given the real parameters of magnitude:

$$0 < A < 1 \tag{10}$$

and GD values:

$$\begin{cases} \tau_l > 0 \\ \tau_h > 0 \\ \tau_{h0} > 0 \\ \tau_0 > 0. \end{cases} \tag{11}$$

Similar to the filter responses, the NGD ones can also be specified with the consideration of the NGD flatness. For this reason, these LP, HP and BP ideal responses depicted in Figs. 2 are defined with the shaded area and also some limitations corresponding to the probable ripple of the NGD value in the NGD bandwidth.

1) NGD CUT-OFF FREQUENCIES AND BANDWIDTHS (BW)

The NGD cut-off angular frequencies of the LP, HP, and BP NGD functions are given by, respectively:

$$\omega_l = 2\pi f_l \tag{12}$$

$$\omega_h = 2\pi f_h \tag{13}$$

and

$$\begin{cases} \omega_a = 2\pi f_a \\ \omega_b = 2\pi f_b. \end{cases} \tag{14}$$

The NGD BWs of LP and BP GD responses are expressed as:

$$\begin{cases} BW_{LP-NGD} = \omega_l \\ BW_{BP-NGD} = \omega_b - \omega_a. \end{cases} \tag{15}$$

There are several ways to define the NGD center frequency related to the BP NGD response. The most practical one is the choice of center frequency with the possibility of analytical expression consideration. Let consider the center frequency defined by:

$$\omega_0 = 2\pi f_0 = \sqrt{\omega_a \omega_b}. \tag{16}$$

2) TF MAGNITUDE

Under this ideal supposition, the LP, HP, and BP VTF magnitudes can be assumed equal to constant:

$$|T(j\omega)| = A \tag{17}$$

where the NGD BWs belongs to the angular frequency ($\omega \in BW_{NGD}$). To simplify the circuit synthesis, we can consider:

- The synthesis of LP NGD circuit can be performed at very low frequencies under the desired magnitude value:

$$T_{LP}(\omega \approx 0) = A. \tag{18}$$

- The BP NGD function around the center frequency, as given in (16):

$$T_{BP}(\omega_0) = A. \tag{19}$$

3) GD VALUES

The NGD cut-off frequencies of LP, HP, and BP TFs are analytically determined by the equations:

$$\begin{cases} GD(\omega_l) = 0 \\ GD(\omega_h) = 0 \\ GD(\omega_a) = 0 \\ GD(\omega_b) = 0. \end{cases} \tag{20}$$

The other equations of the LP, HP and BP NGD circuit syntheses are based on the GDs. At very low frequencies, we denote the GD values of LP and HP NGD functions:

$$\begin{cases} GD_{LP}(\omega \approx 0) = -\tau_l \\ GD_{HP}(\omega \approx 0) = \tau_{h0} \end{cases} \tag{21}$$

The equation related to the BP NGD circuit synthesis is based on the GD at the chosen center frequency:

$$GD(\omega = \omega_0) = -\tau_0. \tag{22}$$

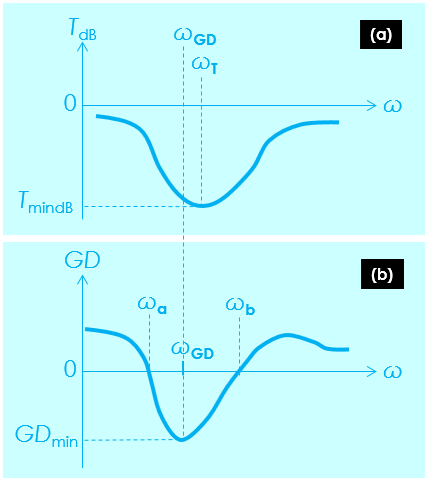

FIGURE 3. Illustration of differences between the optimal frequencies of (a) the magnitude and (b) GD minimal values.

D. OPTIMAL FREQUENCIES OF THE MAGNITUDE AND GD MINIMAL VALUES

Two decade ago, research works revealed that the NGD effect is induced with the absorption of anti-resonant phenomenon [8], [9], [20]–[23], [26]–[29]. Moreover, in the most of NGD circuits studied, the NGD center frequency was assumed as equal to the anti-resonant frequency. By curiosity, we are wondering about deep truth of this statement by proposing the illustrative curves of TF magnitude (defined in equation (5)), shown in Fig. 3(a), and the GD (defined in equation (7)), shown in Fig. 3(b).

From this representation, we denote:

- The optimal frequency related to the magnitude by:

$$\omega_T = 2\pi f_T. \tag{23}$$

  At this frequency, the magnitude should reach its minimal value:

$$\begin{cases} \left.\dfrac{\partial T(\omega)}{\partial \omega}\right|_{\omega=\omega_T} = 0 \\ T_{\min} = T(\omega_T) = T(\omega_0). \end{cases} \tag{24}$$

- The optimal frequency related to the GD is defined by:

$$\omega_{GD} = 2\pi f_{GD}. \tag{25}$$

- The GD at this frequency is defined by:

$$\begin{cases} \left.\dfrac{\partial GD(\omega)}{\partial \omega}\right|_{\omega=\omega_{GD}} = 0 \\ GD_{\min} = GD(\omega_{GD}). \end{cases} \tag{26}$$

So far, various topologies of BP NGD circuits were investigated in the literature [8], [9], [20]–[23], [26]–[29]. However, they are all identified with the typical resonance effect. None of them was designed with inductorless topology. The following section explores the original circuit theory of LP-HP composite inductorless passive cell built with inductorless topology.

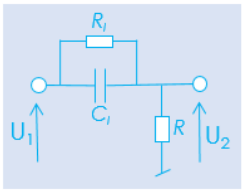

FIGURE 4. Elementary LP NGD passive cell [33].

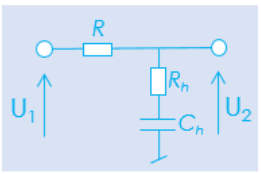

FIGURE 5. Elementary HP passive cell [33].

III. THEORIZATION OF INDUCTORLESS TOPOLOGY WITH THE LP-HP NGD COMPOSITE CONCEPT

The most pragmatic manner to analyze theoretically electronic circuits is based on the TF responses. The analysis depends on the function intended by the circuit. The present section develops the NGD analysis and synthesis of the original inductorless topology under study. The initiated theorization is developed from the TF expression of the LP-HP composite NGD circuit.

A. NGD ANALYSIS OF LP-HP NGD COMPOSITE INDUCTORLESS CELL

The detailed NGD analysis of LP-HP NGD composite cell is elaborated in the present subsection. By dealing with inductorless aspect, the explored circuit is composed of only resistor and capacitor components.

1) ANALYSIS OF LP NGD ELEMENTARY TOPOLOGY CONSTITUTED BY RC-NETWORK

Fig. 4 represents an elementary topology of LP NGD passive circuit comprised of resistors, R and R_l, and capacitors C_l. The key impedance constituting this lumped component cell can be defined by the expression:

$$Z_l(s) = \frac{R_l}{1 + R_l C_l s} \tag{27}$$

The lumped circuit is identified as a system with input voltage, U_1 and output voltage, U_2.

Acting as an L-shape topology, the VTF of RC-network based circuit shown in Fig. 4 can intuitively be determined with the voltage divider principle:

$$T_{LP}(s) = \frac{R}{Z_l(s) + R} \tag{28}$$

The magnitude and NGD values derived from this VTF at very low-frequencies are written as, respectively [31]:

$$T_{LP} = T_{LP}(\omega \approx 0) = \frac{R}{R + R_l} \tag{29}$$

$$GD_{LP} = GD_{LP}(\omega \approx 0) = \frac{-R_l^2 C_l}{R + R_l}. \tag{30}$$

The associated NGD cut-off frequency is expressed as [31]:

$$\omega_l = \frac{\sqrt{R + R_l}}{R_l C_l \sqrt{R}}. \tag{31}$$

We can understand from this formula that the circuit presents $GD_{LP}(\omega < \omega_l) < 0$. Such a GD response belongs to the typical behavior of response shown in Fig. 2(a). Meanwhile, the $R_l C_l$-parallel network-based cell shown in Fig. 4 is classified as a first order LP NGD function.

2) ANALYSIS OF ELEMENTARY HP NGD TOPOLOGY CONSITUTED BY RC NETWORK

Fig. 5 depicts the elementary passive cell dedicated to the HP NGD function. This RC-network is comprised of lumped components of resistors, R and R_h, and capacitor, C_h. The specific impedance to this passive cell is expressed as:

$$Z_h(s) = R_h + \frac{1}{C_h s}. \tag{32}$$

Similar to the previous case, the circuit analysis is referenced by input voltage, U_1, and output voltage, U_2. The associated VTF is equal to:

$$T_{HP}(s) = \frac{Z_h(s)}{R + Z_h(s)}. \tag{33}$$

At very low frequencies($\omega \approx 0$), we can demonstrate that the VTF magnitude and the NGD values are expressed respectively as:

$$T_{HP} = T_{HP}(\omega \approx 0) = 1 \tag{34}$$

$$GD_{HP} = GD_{HP}(\omega \approx 0) = RC_h. \tag{35}$$

We can notice that this GD is always positive, whenever the circuit parameters are. The associated NGD cut-off frequency is written as:

$$\omega_h = \frac{1}{C_h \sqrt{R_h(R + R_h)}}. \tag{36}$$

The GD is literally always negative when $\omega > \omega_h$. Such a behavior belongs to the GD response, shown in Fig. 2(b). Meanwhile, the RC passive cell, introduced in Fig. 5, is classified as a typical HP NGD function.

B. DESCRIPTION OF THE LP-HP NGD COMPOSITE INDUCTORLESS CELL

An original topology of LP-HP NGD composite lumped circuit is inspired from the two previous LP and HP NGD cells. This original passive topology is constituted by $R_l C_l$-parallel and $R_h C_h$-series networks.

1) DESCRIPTION OF THE LP-HP NGD COMPOSITE CELL

The LP-HP NGD composite circuit is constituted by the $R_l C_l$-parallel and the shunt $R_h C_h$-series networks. This circuit is undoubtedly an inductorless topology. The circuit schematic is illustrated in Fig. 6.

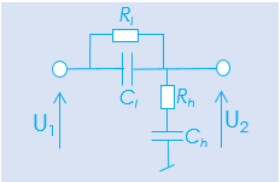

FIGURE 6. Elementary LP-HP NGD composite cell of inductorless topology.

To demonstrate that the LP-HP NGD composite cell behaves as BP NGD topology, we proceed with the VTF elaboration. The VTF of this topology is generally expressed as:

$$T(s) = \frac{Z_h(s)}{Z_l(s) + Z_h(s)} \tag{37}$$

with impedances, Z_l and Z_h expressed in equation (27) and equation (29). After substitution and simplification, the VTF of the LP-HP NGD composite cell can be rewritten in details as:

$$T(s) = \frac{(R_l C_l s + 1)(R_h C_h s + 1)}{R_l C_l R_h C_h s^2 + (R_l C_l + R_l C_h + R_h C_h)s + 1}. \tag{38}$$

We can understand from the previous equation that the inductoless circuit introduced in Fig. 6 is a typical second order linear system. The simplest elementary TF is necessary to identify if a circuit topology can be classified as a BP NGD function. A family of canonical form will be explored in the following paragraph.

2) VTF CANONICAL FORM OF THE PROPOSED LP-HP NGD COMPOSITE TOPOLOGY

The general expression of the canonical form can be derived from the previously introduced VTF. Intuitively, the appropriated canonical form can be written by the fractional formula:

$$T(s) = \frac{s^2 + \omega_n s + \omega_0^2}{s^2 + \omega_d s + \omega_0^2} \tag{39}$$

with the real positive coefficients ω_0, ω_n, and ω_d. The expressions of these coefficient can be obtained by identification with the rational fraction given in equation (38). Accordingly, we have the basic parameters expressed in function of RC network resistor and capacitor values can be formulated as:

$$\omega_0 = \frac{1}{\sqrt{R_l C_l R_h C_h}} \tag{40}$$

$$\omega_n = \frac{1}{R_l C_l} + \frac{1}{R_h C_h} \tag{41}$$

$$\omega_d = \frac{R_l C_l + R_l C_h + R_h C_h}{R_l C_l R_h C_h}. \tag{42}$$

Now, we need to demonstrate analytically why this topology can be classified as a BP NGD function. In the following section, deeper NGD analysis of the composite LP-HP cell proposed in Fig. 6 will be developed in the following section.

IV. BP NGD ANALYSIS AND SYNTHESIS EQUATIONS OF LP-HP COMPOSITE NGD INDUCTORLESS TOPOLOGY

The circuit theoretical analysis and synthesis constitute essential approaches of BP NGD investigation. These approaches serve to understand the typical function appropriated to our inductorless topology introduced in Fig. 6. The analytical investigation on the NGD aspect in function of the $R_l C_l$- and $R_h C_h$ network parameters is developed in the present section.

A. IDENTIFICATION OF INDUCTORLESS TOPOLOGY BP NGD FUNCTION WITH EXPRESSION OF NGD CUT-OFF FREQUENCIES

The existence of NGD cut-off frequencies as specified earlier in Fig. 2(c) constitute one of the unrefutably proof of BP NGD behavior. The present subsection is dedicated to this theoretical demonstration by means of the frequency responses of the TF established in equation (38).

1) ANALYTICAL EXPRESSIONS OF THE FREQUENCY DEPENDENT RESPONSES

The magnitude of our canonical TF can be expressed by means of equation (5). Accordingly, we have the following frequency dependent magnitude:

$$T(\omega) = \frac{\sqrt{(\omega_0^2 - \omega^2)^2 + \omega_n^2 \omega^2}}{\sqrt{(\omega_0^2 - \omega^2)^2 + \omega_d^2 \omega^2}}. \tag{43}$$

The TF phase derived from equation (6) is given by:

$$\varphi(\omega) = \arctan\left(\frac{\omega_n \omega}{\omega_0^2 - \omega^2}\right) - \arctan\left(\frac{\omega_d \omega}{\omega_0^2 - \omega^2}\right). \tag{44}$$

Emphatically, the GD defined in equation (7) becomes:

$$GD(\omega) = \frac{(\omega_d - \omega_n)(\omega^2 + \omega_0^2)}{\left[\omega^4 - (\omega_n \omega_d + 2\omega_0^2)\omega^2 + \omega_0^4\right]} \Big/ \left[\omega^4 + (\omega_n^2 - 2\omega_0^2)\omega^2 + \omega_0^4\right] \Big/ \left[\omega^4 + (\omega_d^2 - 2\omega_0^2)\omega^2 + \omega_0^4\right]. \tag{45}$$

2) NGD ANALYSIS AT PARTICULAR FREQUENCIES

At the frequency $\omega \approx 0$, the magnitude given in equation (43) is equal to $T(\omega \approx 0) = 1$. The GD expressed previously in equation (45) is simplified as:

$$GD(\omega \approx 0) = \frac{\omega_d - \omega_n}{\omega_0^2}. \tag{46}$$

At the frequency $\omega = \omega_0$, the magnitude of TF is transformed as:

$$T(\omega_0) = \frac{\omega_n}{\omega_d}. \tag{47}$$

Then, the GD expressed previously in equation (45) can be simplified as:

$$GD(\omega_0) = \frac{2(\omega_n - \omega_d)}{\omega_n \omega_d}. \tag{48}$$

It can be underlined from this last equation that when:

$$\omega_n < \omega_d \tag{49}$$

the LP-HP composite circuit generate an NGD at $\omega = \omega_0$. Under this condition, equation (46) proves that the GD is positive at $\omega \approx 0$. Because of the variation of GD from positive value (at very low frequencies) to negative value at $\omega = \omega_0$, the cut-off frequencies should belong between 0 and ω_0.

3) NGD CUT-OFF FREQUENCIES

We remind that the NGD cut-off frequencies associated to any TF are the roots of the GD as defined in equation (9). In the present case of study, we have the GD expressed as in (45). It was stated that the NGD cut-off frequencies are the root of equation (9). Meanwhile, the NGD cut-off frequencies are also the root of numerator of the GD given in (45) which is the root of $\omega^4-(\omega_n\omega_d+2\omega_0^2)\omega^2+\omega_0^4=0$. Subsequently, we can demonstrate that our GD contains two cut-off frequencies, which can be formulated as:

$$\omega_a = \sqrt{\omega_0^2 + \frac{\omega_n\omega_d - \sqrt{\omega_n\omega_d(4\omega_0^2+\omega_n\omega_d)}}{2}} \tag{50}$$

$$\omega_b = \sqrt{\omega_0^2 + \frac{\omega_n\omega_d + \sqrt{\omega_n\omega_d(4\omega_0^2+\omega_n\omega_d)}}{2}}. \tag{51}$$

The NGD cut-off frequencies of these two expressions satisfy relation (16). It can be understood that when $\omega_a < \omega < \omega_b$, we have $GD(\omega) < 0$. It means that the GD response belongs to the case of response figured out in Fig. 2(c). In a nutshell, the combination of LP and HP composite topology exposed in Fig. 6 belongs to the BP NGD function classification.

4) NGD ANALYSIS IN FUNCTION OF THE LP-HP RC PARAMETERS

The magnitude and GD of the TF, given in equation (47) and in equation (48), respectively, can be expressed in function of the LP-HP RC parameters. Substituting the expressions of ω_0 in equation (40), ω_n in equation (41), and ω_d in equation (42), into the magnitude defined in equation (17), we have:

$$A = \frac{R_lC_l + R_hC_h}{R_lC_l + R_lC_h + R_hC_h}. \tag{52}$$

The identical mathematical operation applied to the GD given in equation (22) enables to express:

$$\tau_0 = \frac{2R_hC_lR_l^2C_h^2}{(R_lC_l + R_hC_h)(R_lC_l + R_lC_h + R_hC_h)}. \tag{53}$$

Before the elaboration of the design equations from these analytical relations, a numerical investigation about the comparison of the TF magnitude and GD optimal frequencies will be explored in the next section.

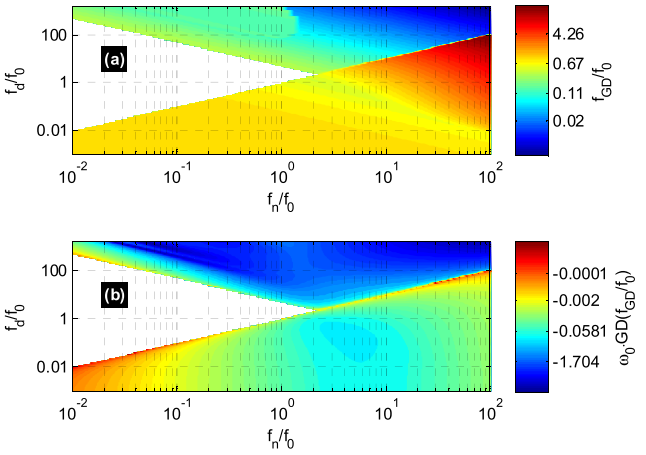

FIGURE 7. Mappings of (a) GD optimal frequency and (b) product between the magnitude optimal frequency and optimal GD value loglog x- and y-axes.

B. COMPARISON OF THE OPTIMAL FREQUENCIES OF TF MANITUDE AND GD MINIMUMS OF THE LP-HP COMPOSITE TOPOLOGY

In many of BP NGD circuit design study, the optimal or anti-resonance frequencies related to the magnitude and related to the GD were assumed as identical. The present numerical investigation aims to illustrate their differences in function of the parameters of the canonical form expressed in equation (39).

1) MAPPING OF THE GD OPTIMAL FREQUENCY VERSUS CANONICAL FORM TF PARAMETERS

The present mapping numerical investigation is based on the consideration of the GD analytical expression introduced in equation (45). The x- and y-axes are represented by the variation of the denominator normalized frequency f_n/f_0 versus the numerator f_d/f_0. The calculations were performed with f_n/f_0 varied from 0.01 to 100 whereas f_d/f_0 is varied from 0.001 and 1000.

The cartography of the ratio f_{GD}/f_0 is mapped in Figs. 7(a). This numerical result enables to state that for any BP NGD function defined by the canonical TF introduced in equation (38), we have:

$$f_0 \neq f_{GD}. \tag{54}$$

By considering the GD given in equation (45), we can calculate its product with the magnitude optimal frequency

$$\xi = \omega_0 \cdot GD(f_{GD}/f_0). \tag{55}$$

The obtained result is displayed in Fig. 7(b). It can be seen that the GD cannot be negative in the certain zone represented by the triangle area under loglog plots of x- and y-axes.

2) RELATION BETWEEN THE TF CANONICAL FORM NUMERATOR AND DENOMINATOR COEFFICIENTS AT GD(F)=0

To accurately identify the limit of NGD zone, the variation of the denominator normalized frequency f_d/f_0 versus the

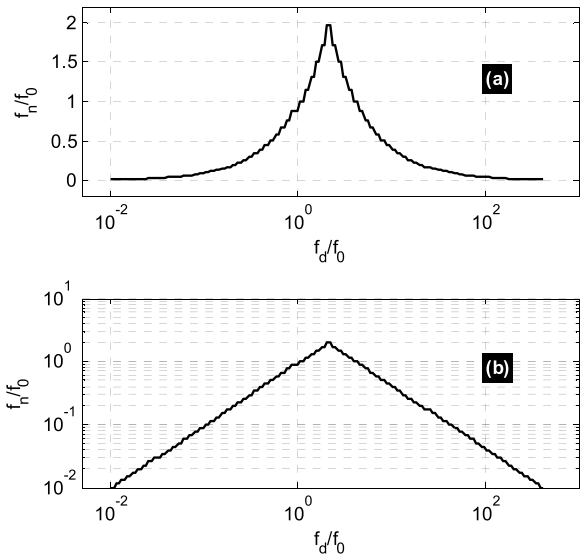

FIGURE 8. Variation of denominator and numerator BP TF parameters normalized with the TF magnitude optimal frequency: (a) linear and (b) loglog plots.

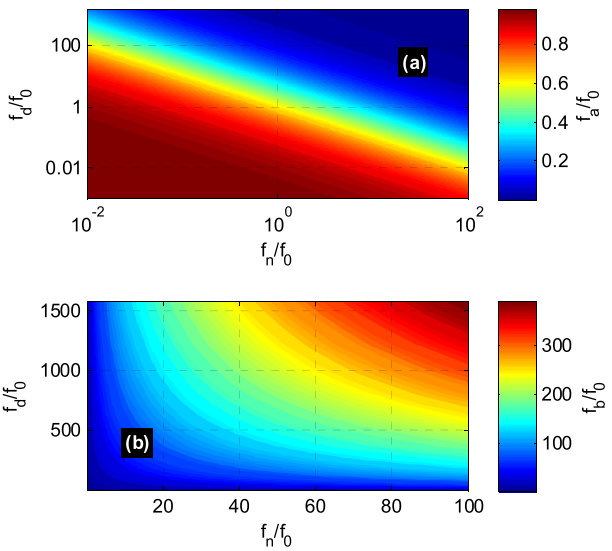

FIGURE 9. Mappings of lower cut-off frequencies of BP NGD function versus normalized numerator and denominator parameters in (a) loglog and (b) in linear x- and y-axes.

numerator f_n/f_0 was also calculated from equation (16) by means of GD expressed in equation (45). Doing this, the normalized value of f_d/f_0 was swept from 0.01 to 2. Therefore, we obtain the abacus of Figs. 8. In this range of value, the maximal value of the numerator is slightly lower than 2. It can be seen that a numerator parameter value corresponds to two different values of denominator ones. In the present case of study, we have singular behavior at the canonical form parameters at $f_n = 2.071f_0$ and $f_d = 1.968f_0$.

3) MAPPING OF THE CUT-OFF FREQUENCIES FREQUENCY VERSUS CANONICAL FORM TF PARAMETERS

The cartographies in Fig. 9(a) and Fig. 9(b) represent the mappings of the normalized cut-off frequencies, f_a/f_0 and f_b/f_0 as function of $(f_d/f_0, f_n/f_0)$. It can be seen that f_a/f_0 is decreasing when f_d/f_0 and f_n/f_0 increase. However, we have an inverse effect for f_b/f_0, which is increasing when f_d/f_0 and f_n/f_0 increase.

C. DESIGN AND SYNTHESIS EQUATIONS OF LP-HP NGD COMPOSITE CIRCUIT

We recall that the four main parameters of our BP NGD circuit shown in Fig. 6 are R_l, C_l, R_h, and C_h. To determine these parameters, the desired BP NGD specifications as the resonance frequency, ω_0, the attenuation, $0 < A < 1$, and the GD, $\tau_0 > 0$ must be initially chosen. Knowing this BP NGD targeted objective, we can use the synthesis design equations of the LP-HP NGD composite circuit to be introduced in the following paragraphs.

1) FORMULATIONS OF THE RESISTOR AND CAPACITOR COMPONENTS IN FUNCTION OF THE DESIRED BP NGD SPECIFICATIONS

By inverting the system of equation (47) and equation (48) given the attenuation, A, and the delay, τ_0, we have the synthesis formulas of the TF canonical form numerator and denominator coefficients:

$$\omega_n = \frac{2(1-A)}{\tau_0} \tag{56}$$

$$\omega_d = \frac{2(1-A)}{A\ \tau_0}. \tag{57}$$

The determination of the RC components values can be performed under LP, HP, and BP NGD response specifications:

$$\tau_l = \frac{1 - A - \sqrt{(\omega_0\tau_0)^2 - (1-A)^2}}{\omega_0^2\tau_0} \tag{58}$$

$$\tau_h = \frac{\tau_0\tau_l}{2\tau_l(1-A) - \tau_0} \tag{59}$$

$$\tau_{lh} = \frac{2\tau_l^2(1-A)^2}{A\,[2\tau_l(1-A) - \tau_0]}. \tag{60}$$

Therefore, by solving the equation related to the time constant delay, we can establish the following relations:

$$C_h = \frac{\tau_h}{R_h} \tag{61}$$

$$R_l = \frac{R_h\tau_{lh}}{\tau_h} \tag{62}$$

$$C_l = \frac{\tau_l\tau_h}{R_h\tau_{lh}} \tag{63}$$

by choosing an arbitrary value of R_h. It can be emphasized form these equations that all values of parameters of the cell introduced in Fig. 6 enables to generate the BP NGD function.

2) BP NGD EXISTENCE CONDITION WITH RESPECT TO THE EXPECTED BP NGD SPECIFICATIONS

Now, we can express the cut-off frequencies associated to the resonance frequency, ω_0, the attenuation, A, and the delay, τ_0. This simplification can be performed by considering the expressions of canonical parameters, given in equation (56)

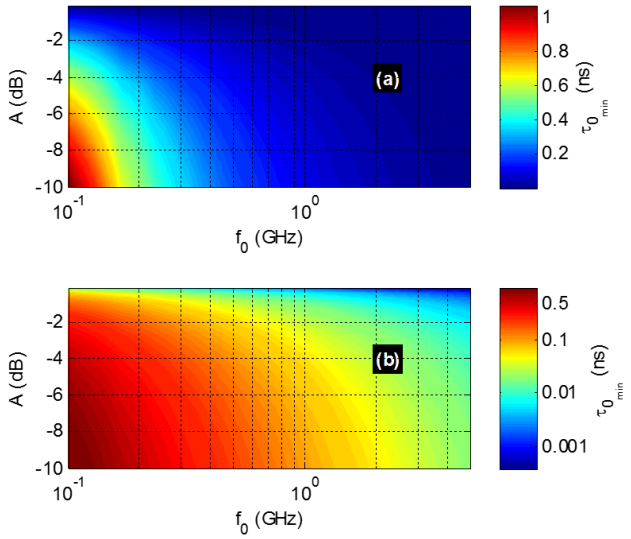

FIGURE 10. Cartographies of τ_{0min} versus (A,f_0) in (a) linear and (b) logarithmic bar scale.

and equation (57) into equation (50) and equation (51). Consequently, we have the cut-off frequencies:

$$\omega_a = \sqrt{\frac{(1-A)^2}{A^2\tau_0^2} + \frac{\omega_0^2}{2A} - \frac{(1-A)}{A\tau_0^2}\sqrt{\omega_0^2 + \frac{(1-A)^2}{A\tau_0^2}}} \quad (64)$$

$$\omega_b = \sqrt{\frac{(1-A)^2}{A^2\tau_0^2} + \frac{\omega_0^2}{2A} + \frac{(1-A)}{A\tau_0^2}\sqrt{\omega_0^2 + \frac{(1-A)^2}{A\tau_0^2}}}. \quad (65)$$

The existence of the NGD cut-off frequencies depends on the sign of the quantities in the argument of root square of equation (58). The following paragraph will define the analytical condition of BP NGD existence condition.

3) BP NGD EXISTENCE CONDITION WITH RESPECT TO THE EXPECTED BP NGD SPECIFICATIONS

The theoretical design equation established in the previous paragraph depend on the specifications choice. The synthesis equation does not work for all value of ω_0, A, an τ_0. Knowing that R_l, C_l, and C_h are real positive, the existence condition is analytically expressed as:

$$\omega_0\tau_0 \geq 1 - A. \quad (66)$$

Otherwise, we have the minimal value:

$$\tau_{0\,\min} = \frac{1-A}{\omega_0}. \quad (67)$$

Figs. 10 illustrate the linear and logarithmic mapping plots of the minimal GD. This cartography corresponds to the variations of A between -10 dB and -0.1 dB and f_0 from 0.1 GHz to 5 GHz. We can see that the minimal GD decreases from 1.1 ns to 0.4 ps in the considered range of values.

To validate the developed LP-HP NGD composite circuit theory, a comparison between calculated, simulated, and experimental results will be discussed in the following section.

TABLE 1. Physical parameters of the substrate.

Structure	Description	Parameters	Values
Substrate	Relative permittivity	ε_r	4.5
	Loss tangent	$\tan(\delta)$	0.02
	Thickness	h	1.6 mm
Metallization conductor	Copper conductivity	σ	58 MS/s
	Thickness	t	35 µm

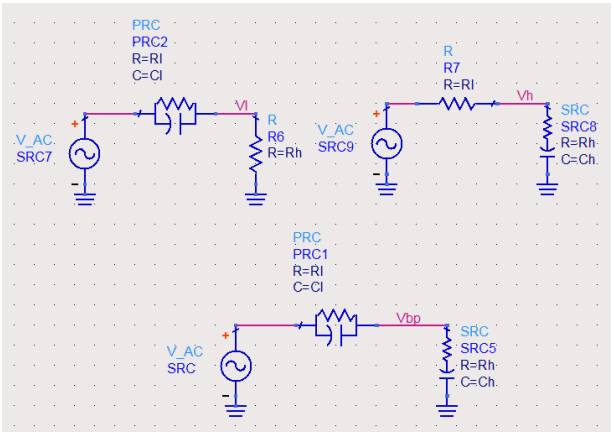

FIGURE 11. Design schematic of the simulated LP, HP and LP-HP NGD circuit.

V. MESAUREMENT TESTS OF LP-HP COMPOSITE NGD INDUCTORLESS CIRCUITS AND BP NGD FUNTION VALIDATION RESULTS

The present section deals with the validation of the previous theory of inductorless BP NGD topology. The design and fabrication of inductorless circuit PoCs will be described. Then, the calculated, simulated and simulated results will be discussed. The calculations were performed with the Matlab programming of the PoC VTFs. The simulation results discussed in the present section were run in the schematic environment of the electronic and RF/microwave circuit simulator ADS®from Keysight Technologies®.

A. DESCRIPTION OF LP-HP NGD COMPOSITE PROTOTYPES

The PoCs of considered inductorless BP NGD circuits were designed for the validation. These PoCs were implemented on Cu-metalized FR4 dielectric substrate in hybrid technology. The substrate physical characteristics are addressed in Table 1.

The circuit designs were performed with the application of synthesis equations (61), (62), and (63), respectively. The NGD circuit prototypes were designed and fabricated. Fig. 11 shows the schematics of the designed LP, HP, and LP-HP NGD composite circuits. The electrical parameters of PoC_1 and PoC_2 are indicated in Table 2.

The photographs of the fabricated LP-HP NGD composite $prototype_1$ and $prototype_2$ are displayed in Fig. 12(a) and

TABLE 2. Parameters of the NGD PoC_1 and PoC_2.

Description		Parameter	Nominal value
PoC_1	Specifications	Center frequency	f_0=22 MHz
		NGD value	τ_0=2.5 ns
		Attenuation	A=-6 dB
	Calculated NGD circuit parameters	Resistor	R_h=68 Ω
			R_l=100 Ω
		Capacitor	C_l=33 pF
			C_h=100 pF
PoC_2	Specifications	Center frequency	f_0=13.5 MHz
		NGD value	τ_0=5 ns
		Attenuation	A=-6 dB
	Calculated NGD circuit parameters	Resistor	R_h=68 Ω
			R_l=150 Ω
		Capacitor	C_l=33 pF
			C_h=150 pF

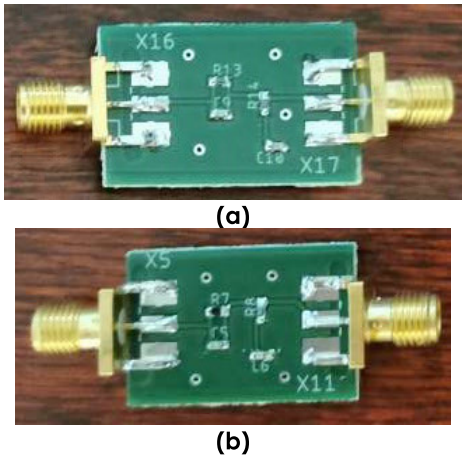

FIGURE 12. Photographs of the fabricated LP-HP NGD (a) $prototypes_1$ and (b) $prototypes_2$.

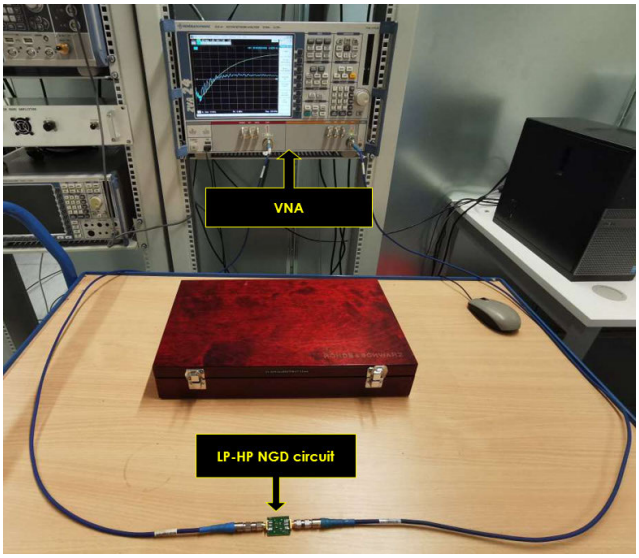

FIGURE 13. LPHP NGD prototype experimental setup photograph.

in Fig. 12(b), respectively. These prototypes present physical sizes, 29 mm × 18 mm and 26 mm × 17 mm, respectively.

B. DISCUSSION ON THE VALIDATION RESULTS

The validations of the LP-HP composite NGD topologies are explored in the present subsection. The simulation and experimental validations of the LP-HP composite NGD topologies are explored in the present subsection.

1) EXTRACTION OF EXPERIMENTED VTF

The measurement of the inductorless NGD circuit VTF magnitude and GD were carried out indirectly from two-port frequency dependent S-parameters. Figs. 13 highlight the experimental setup photograph. The measured data were recorded in touchstone format. The tests were realized with a Vector Network Analyzer (VNA) Rohde & Schwarz®referenced ZVA 24 and specified by frequency band from 10 MHz to 24 GHz. The measured VTF magnitude and GD of the tested circuits were extracted from S-parameter to VTF transform relation. Comparisons between the calculated ("Calc.") and simulated ("Sim.") results in the frequency band from 100 kHz to 0.1 GHz with ADS®, and measured ("Meas.") results in the frequency band from 10 MHz to 0.1 GHz will be discussed in the following paragraphs.

2) RESULTS OF LP-HP NGD COMPOSITE POC_1

The calculated, simulated, and measured VTF GDs of the LP, HP and LP-HP composite NGD PoC_1 are plotted in Figs. 14. Those of the associated VTF magnitudes are displayed in Figs. 15.

It can be pointed out that these comparative results present a very good agreement. Table 3 presents the comparison of NGD specifications. As expected in Fig. 14(a), the LP NGD cell exhibits a cut-off frequency of about $f_{LP} = 75.4$ MHz. While the HP NGD cell cut-off frequency is of about $f_{HP} = 14.67$ MHz as seen in Fig. 14(b). The VTF magnitude of LP is increasing with frequency, while the HP one is decreasing. The calculated, simulated, and measured GDs of LP-HP composite circuit are introduced in Fig. 14(c). More importantly, it can be found that they are in very good agreement.

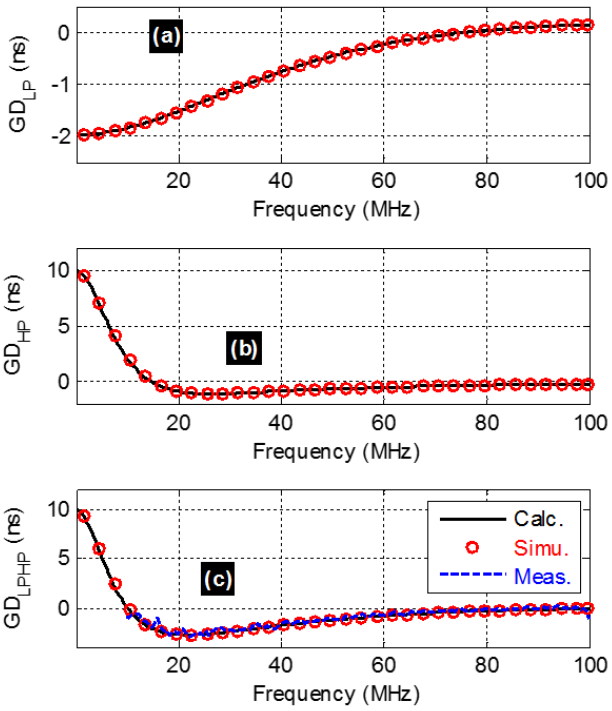

FIGURE 14. Comparisons of calculated, simulated, and measured VTF GD of (a) LP, (b) HP, and (b) LP-HP composite NGD prototype$_1$.

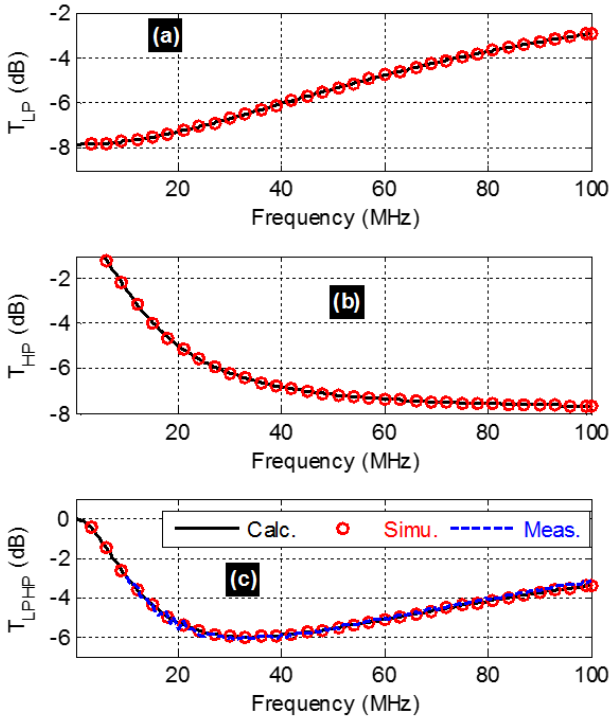

FIGURE 15. Comparisons of calculated, simulated, and measured VTF magnitude of (a) LP, (b) HP, and (b) LP-HP composite prototype$_1$.

As expected, in the working frequency band, the LP-HP composite circuit PoC$_1$ behaves as a BP NGD function. The NGD center frequency of approximately $f_{GD} = 21.75$ MHz against

TABLE 3. Comparison of LP and HP NGD prototype specifications.

Function	Approach	f_{LP}	$GD_{LP}(0)$	$T_{LP}(0)$
LP	Calc.	75.44 MHz	-1.964 ns	-7.86 dB
	Simu.	75 MHz	-1.96 ns	-7.86 dB
Function	Approach	f_{HP}	$GD_{HP}(0)$	$T_{HP}(f_{HP})$
HP	Calc.	14.67 MHz	9.98 ns	-7.66 dB
	Simu.	14.2 MHz	9.5 ns	-7.65 dB

Approach	f_{GD}	$GD(f_{GD})$	BW	f_o	$T(f_o)$
Calc.	21.75 MHz	-2.21 ns	89.91 MHz	33.4 MHz	-5.97 dB
Simu.	21.5 MHz	-2.15 ns	89.5 MHz	33.2 MHz	-5.9 dB
Meas.	22.2 MHz	-2.8 ns	-	31.5 MHz	-6.1 dB

TABLE 4. Comparison of BP NGD prototype specifications.

Function	Approach	f_{LP}	$GD_{LP}(0)$	$T_{LP}(0)$
LP	Calc.	57.54 MHz	-3.4 ns	-10.118 dB
	Simu.	57 MHz	-3.39 ns	-10.12 dB
Function	Approach	f_{HP}	$GD_{HP}(0)$	$T_{HP}(f_{HP})$
HP	Calc.	8.42 MHz	22.35 ns	-10 dB
	Simu.	8.48 MHz	22.4 ns	-10 dB

Approach	f_{GD}	$GD(f_{GD})$	BW	f_o	$T(f_o)$
Calc.	13.4 MHz	-3.915 ns	75.76 MHz	22.58 MHz	-7.907 dB
Simu.	13.1 MHz	-3.964 ns	76 MHz	21.5 MHz	-7.89 dB
Meas.	16.4 MHz	-4.8 ns	-	20.1 MHz	-8.16 dB

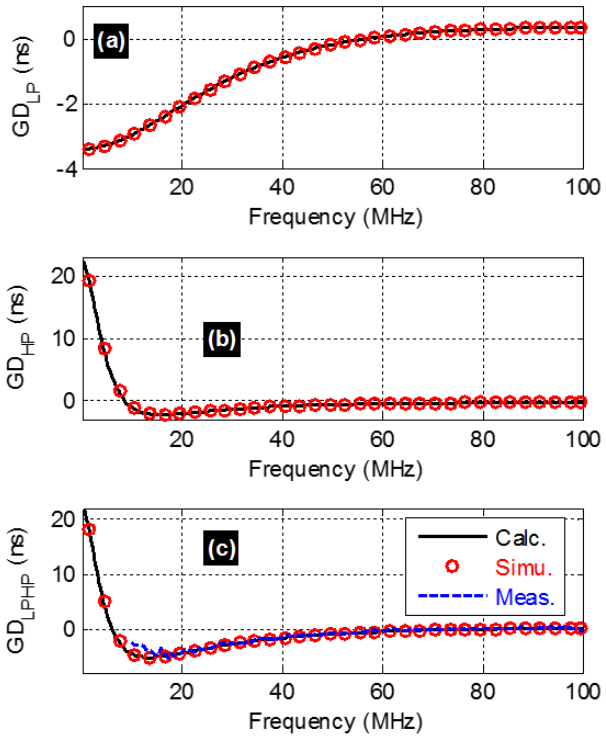

FIGURE 16. Comparisons of calculated, simulated, and measured VTF GD of (a) LP, (b) HP, and (b) LP-HP composite NGD prototype$_2$.

the optimal frequency of VTF magnitude $f_0 = 33.4$ MHz, as indicated in Table 3. This confirms the shift between the

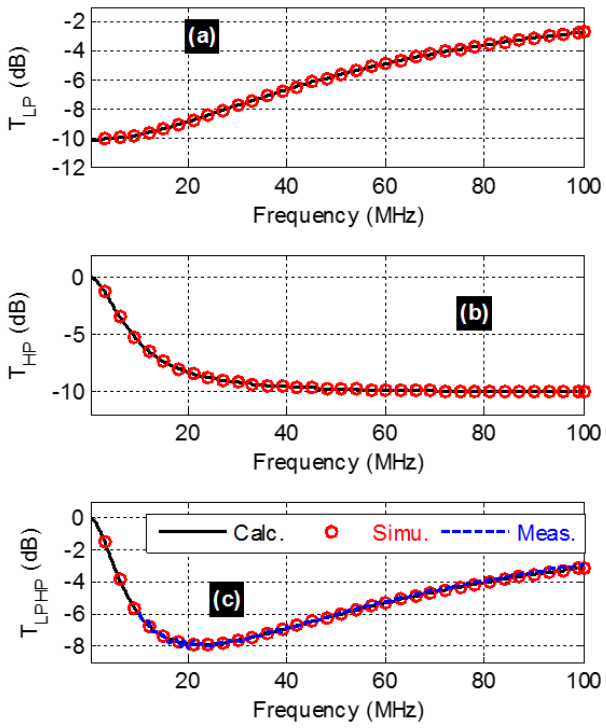

FIGURE 17. Comparisons of calculated, simulated, and measured VTF magnitude of (a) LP, (b) HP, and (b) LP-HP composite NGD prototype$_2$.

GD and magnitude optimal frequencies identified in paragraph IV-B-1. The LP-HP composite VTF attenuation at $f = f_{GD}$ is about 6 dB.

3) RESULTS OF LP-HP NGD COMPOSITE POC$_2$

Similar to the previous results of PoC$_1$, as shown in Figs. 16, the calculated, simulated, and measured GDs of the NGD LP, HP, and LP-HP composite PoC$_2$ are in excellent correlation. The NGD circuit magnitudes are compared in Figs. 17. Table 4 summarizes the NGD specifications of PoC$_2$. As expected in Fig. 16(a) and Fig. 16(b), in this case, the LP and HP NGD cut-off frequencies are around $f_{LP} = 57.54$ MHz and $f_{HP} = 8.42$ MHz. Once again, the LP-HP NGD composite GD result of Fig. 16(c) confirms the BP NGD behavior around center frequency of approximately $f_{GD} = 13.4$ MHz. As seen in Table 4, the magnitude and GD optimal frequencies present a ratio of about $f_0/f_{GD} \approx 1.6$. It can be seen from Fig. 17(c) that the LP-HP composite VTF attenuation is of about 7.8 dB.

The overall results of present study upholds that the BP NGD function can be implemented with inductorless passive circuit.

VI. CONCLUSION

An original theory of inductorless BP NGD topology is investigated. The passive topology is implemented only with resistor and capacitor components. After the NGD function specification, NGD analyses of LP and HP cells are introduced is elaborated. Then, the theoretical characterization of LP-HP NGD composite cell. The canonical VTF of the BP NGD topology serve to determine the constituting RC-network parameter in function of the desired BP NGD specifications.

The effectiveness of the developed inductorless BP NGD theory is validated with PoCs and prototypes implemented in hybrid topology. As expected, the calculation, simulation, and measurement results are in very good correlation. It was found that the shift between the optimal frequencies related to the GD and VTF magnitude minimal values. In the next step of the study, the inductorless topology will be modelled based on S-matrix approach in order to take into account the reflection effect. Comparisons with the existing NGD circuit with particular attention on the reflection aspect as performed in [24], [34] will be investigated.

The developed LP-HP NGD composite cell is very useful for the RF and microwave applications where the miniature NGD circuits are necessary. The identification of the BP NGD topologies without inductor enables to overcome the limitation of NGD circuit integration caused by the self-inductance. The developed topologies present a flexibility for the reconfigurability and the potential integration in the RF and microwave circuits [35], [36].

REFERENCES

[1] G. Groenewold, "Noise and group delay in active filters," *IEEE Trans. Circuits Syst. I, Reg. Papers*, vol. 54, no. 7, pp. 1471–1480, Jul. 2007.
[2] S.-S. Myoung, B.-S. Kwon, Y.-H. Kim, and J.-G. Yook, "Effect of group delay in RF BPF on impulse radio systems," *IEICE Trans. Commun.*, vol. 90, no. 12, pp. 3514–3522, 2007.
[3] I. C. Hunter, *Theory and Design of Microwave Filters* (IET Electromagnetic Waves Series 48), P. J. B. Clarricoats and E. V. Jull, Eds. Cambridge, U.K.: Cambridge Univ. Press, 2006.
[4] J.-S. Hong and M. J. Lancaster, *Microstrip Filters for RF/Microwave Applications*. New York, NY, USA: Wiley, 2001.
[5] G. Jang and S. Kahng, "Design of a dual-band metamaterial bandpass filter using zeroth order resonance," *Prog. Electromagn. Res. C*, vol. 7, pp. 149–162, 2009.
[6] G. Jang and S. Kahng, "Design of a metamaterial bandpass filter using the ZOR of a modified circular mushroom structure," *Microw. J.*, vol. 54, no. 5, pp. 158–167, May 2011.
[7] G. Jang and S. Kahng, "Compact metamaterial zeroth-order resonator bandpass filter for a UHF band and its stopband improvement by transmission zeros," *IET Microw., Antennas Propag.*, vol. 5, no. 10, pp. 1175–1181, Jul. 2011.
[8] G. V. Eleftheriades, O. Siddiqui, and A. K. Iyer, "Transmission line for negative refractive index media and associated implementations without excess resonators," *IEEE Microw. Wireless Compon. Lett.*, vol. 13, no. 2, pp. 51–53, Feb. 2003.
[9] O. F. Siddiqui, M. Mojahedi, and G. V. Eleftheriades, "Periodically loaded transmission line with effective negative refractive index and negative group velocity," *IEEE Trans. Antennas Propag.*, vol. 51, no. 10, pp. 2619–2625, Oct. 2003.
[10] S. Chu and S. Wong, "Linear pulse propagation in an absorbing medium," *Phys. Rev. Lett.*, vol. 48, pp. 738–741, Mar. 1982.
[11] B. Ségard and B. Macke, "Observation of negative velocity pulse propagation," *Phys. Lett. A*, vol. 109, pp. 213–216, May 1985.
[12] B. Macke and B. Ségard, "Propagation of light-pulses at a negative group-velocity," *Eur. Phys. J. D*, vol. 23, no. 1, pp. 125–141, Apr. 2003.
[13] M. W. Mitchell and R. Y. Chiao, "Negative group delay and 'fronts' in a causal system: An experiment with very low frequency bandpass amplifiers," *Phys. Lett. A*, vol. 230, nos. 3–4, pp. 133–138, Jun. 1997.
[14] M.-E. Hwang, S.-O. Jung, and K. Roy, "Slope interconnect effort: Gate-interconnect interdependent delay modeling for early CMOS circuit simulation," *IEEE Trans. Circuits Syst. I, Reg. Papers*, vol. 56, no. 7, pp. 1428–1441, Jul. 2009.

[15] K.-P. Ahn, R. Ishikawa, and K. Honjo, "Group delay equalized UWB InGaP/GaAs HBT MMIC amplifier using negative group delay circuits," *IEEE Trans. Microw. Theory Techn.*, vol. 57, no. 9, pp. 2139–2147, Sep. 2009.
[16] B. Ravelo, S. Lalléchère, A. Thakur, A. Saini, and P. Thakur, "Theory and circuit modeling of baseband and modulated signal delay compensations with low- and band-pass NGD effects," *AEU-Int. J. Electron. Commun.*, vol. 70, no. 9, pp. 1122–1127, Sep. 2016.
[17] L.-F. Qiu, L.-S. Wu, W.-Y. Yin, and J.-F. Mao, "Absorptive band-stop filter with prescribed negative group delay and bandwidth," *IEEE Microw. Wireless Compon. Lett.*, vol. 27, no. 7, pp. 639–641, Jul. 2017.
[18] T. Shao, Z. Wang, S. Fang, H. Liu, and Z. N. Chen, "A full-passband linear-phase band-pass filter equalized with negative group delay circuits," *IEEE Access*, vol. 8, pp. 43336–43343, Feb. 2020.
[19] C. D. Broomfield and J. K. A. Everard, "Broadband negative group delay networks for compensation of oscillators, filters and communication systems," *Electron. Lett.*, vol. 36, no. 23, pp. 1931–1933, Nov. 2000.
[20] A. Mortazawi and W. Alomar, "Negative group delay circuit," U.S. Patent 0 093 958, Mar. 31, 2016.
[21] H. Mirzaei and G. V. Eleftheriades, "Realizing non-Foster reactive elements using negative-group-delay networks," *IEEE Trans. Microw. Theory Techn.*, vol. 61, no. 12, pp. 4322–4332, Dec. 2013.
[22] T. Zhang, R. Xu, and C.-T.-M. Wu, "Unconditionally stable non-foster element using active transversal-filter-based negative group delay circuit," *IEEE Microw. Wireless Compon. Lett.*, vol. 27, no. 10, pp. 921–923, Oct. 2017.
[23] Z. Wang, Y. Cao, T. Shao, S. Fang, and Y. Liu, "A negative group delay microwave circuit based on signal interference techniques," *IEEE Microw. Wireless Compon. Lett.*, vol. 28, no. 4, pp. 290–292, Apr. 2018.
[24] M. A. Sanchez-Soriano, J. Dura, S. Sirci, and S. Marini, "Signal-interference-based structure with negative group delay properties," in *Proc. 48th Eur. Microw. Conf. (EuMC)*, Sep. 2018, pp. 1021–1024.
[25] M. Kandic and G. E. Bridges, "Asymptotic limits of negative group delay in active resonator-based distributed circuits," *IEEE Trans. Circuits Syst. I, Reg. Papers*, vol. 58, no. 8, pp. 1727–1735, Aug. 2011.
[26] C.-T.-M. Wu and T. Itoh, "Maximally flat negative group-delay circuit: A microwave transversal filter approach," *IEEE Trans. Microw. Theory Techn.*, vol. 62, no. 6, pp. 1330–1342, Jun. 2014.
[27] G. Liu and J. Xu, "Compact transmission-type negative group delay circuit with low attenuation," *Electron. Lett.*, vol. 53, no. 7, pp. 476–478, Mar. 2017.
[28] T. Shao, Z. Wang, S. Fang, H. Liu, and S. Fu, "A compact transmission line self-matched negative group delay microwave circuit," *IEEE Access*, vol. 5, no. 1, pp. 22836–22843, Oct. 2017.
[29] G. Chaudhary, Y. Jeong, and J. Lim, "Miniaturized dual-band negative group delay circuit using dual-plane defected structures," *IEEE Microw. Wireless Compon. Lett.*, vol. 21, no. 1, pp. 19–21, Jan. 2011.
[30] T. Shao, S. Fang, Z. Wang, and H. Liu, "A compact dual-band negative group delay microwave circuit," *Radioengineering*, vol. 27, no. 4, pp. 1070–1076, Dec. 2018.
[31] B. Ravelo, "Similitude between the NGD function and filter gain behaviours," *Int. J. Circuit Theory Appl.*, vol. 42, no. 10, pp. 1016–1032, Oct. 2014.
[32] B. Ravelo, "First-order low-pass negative group delay passive topology," *Electron. Lett.*, vol. 52, no. 2, Jan. 2016, pp. 124–126.
[33] B. Ravelo, "High-pass negative group delay RC-network impedance," *IEEE Trans. Circuits Syst. II, Exp. Briefs*, vol. 64, no. 9, pp. 1052–1056, Sep. 2017.
[34] R. Gomez-Garcia, J.-M. Munoz-Ferreras, W. Feng, and D. Psychogiou, "Input-reflectionless negative-group-delay bandstop-filter networks based on lossy complementary duplexers," in *IEEE MTT-S Int. Microw. Symp. Dig.*, Boston, MA, USA, Jun. 2019, pp. 1031–1034.
[35] R. Gomez-Garcia and J. I. Alonso, "Systematic method for the exact synthesis of ultra-wideband filtering responses using high-pass and low-pass sections," *IEEE Trans. Microw. Theory Techn.*, vol. 54, no. 10, pp. 3751–3764, Oct. 2006.
[36] M. Fan, K. Song, and Y. Fan, "Reconfigurable low-pass filter with sharp roll-off and wide tuning range," *IEEE Microw. Wireless Compon. Lett.*, vol. 30, no. 7, pp. 649–652, Jul. 2020.

BLAISE RAVELO (Member, IEEE) is currently a University Full Professor with NUIST, Nanjing, China. His research interests include multiphysics and electronics engineering. He is also a pioneer of the Negative Group Delay (NGD) concept about $t<0$ signal travelling physical space. This extraordinary concept is potentially useful for anticipating and prediction all kind of information. He was a Research Director of ten Ph.D. students (seven defended), postdoctoral researchers, research engineers, and master's internships. With U.S., Chinese, Indian, European, and African partners, he is actively involved and contributes on several international research projects (ANR, FUI, FP7, INTERREG, H2020, Euripides^2, and Eurostars…). He is a member of *IET Electronics Letters* Editorial Board as a Circuit and System Subject Editor. He has been a member of Scientific Technical Committee of Advanced Electromagnetic Symposium (AES) since 2013. His Google scholar H-index in 2020 is 21. He is a member of research groups: IEEE, URSI, GDR Ondes, Radio Society and (co-) authors of more than 270 scientific research articles in new technologies published in international conference and journals. He is a Lecturer on circuit and system theory, science, technology, engineering, and maths (STEM), and applied physics. He is regularly invited to review articles submitted for publication to international journals (IEEE TRANSACTIONS ON MICROWAVE THEORY AND TECHNIQUES, IEEE TRANSACTIONS ON CIRCUITS AND SYSTEMS, IEEE TRANSACTIONS ON ELECTROMAGNETIC COMPATIBILITY, IEEE TRANSACTIONS ON INDUSTRIAL ELECTRONICS, IEEE ACCESS, IET CDS, and IET MAP) and books (Wiley and Intech Science).

SAMUEL NGOHO is graduated from ESIGELEC, Rouen, France, in 2012. He received the Ph.D. degree in thematic of high-frequency electronics, photonics, and systems from the XLIM Laboratory, University of Limoges, Limoges, France. His Ph.D. subject concerned was based on the design and production of integrated optoelectronic components for high-speed telecommunications systems. He worked as an Integration, Verification, Validation, and Qualification Engineer of RF / HF products and systems for civil and military applications. He works as a System Engineer with THALES SIX, Gennevilliers, France. His research interests include microelectronics, in particular in the development of innovative functions integrated in microwave devices to meet the need for densification and evolution of spectra for future communications systems. He also takes part within research groups in the use of unfamiliar methods for resolving complex system as Kron's method. He is currently a member of The French Association Science for Cognitive, Cybernetics, and Technical Systems, Association Française de science des systems Cybernétiques (AFSET), ENSAM, Paris.

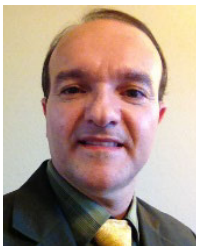

GLAUCO FONTGALLAND (Senior Member, IEEE) was born in Fortaleza, CE, Brazil, in March 1966. He received the degree and the M.S. degree in electrical engineering from the Universidade Federal de Campina Grande (UFCG), Campina Grande, Brazil, 1990 and 1993, respectively, and the Ph.D. degree in electronics from the Toulouse Institut National Polytechnique–ENSEEIHT, Toulouse, France, in 1999.

From 2010 to 2012, he was Visiting Scholar with the ElectroScience Laboratory, The Ohio State University, Columbus, OH, USA. He is currently a Full Professor with the Universidade Federal de Campina Grande (UFCG), Campina Grande, Brazil, where he develops research on: electromagnetic modeling, EMC, EMI, ESD, RFID, UWB, propagation, and antennas for various applications. He has published more than 200 papers in journal and conferences.

Dr. Fontgalland is the past IEEE AP-S chapter chair and a member of the 2020 IEEE AP-S student design contest and 2020 IEEE AP-S Field awards Evaluation. His Thesis work was nominated for the Leopold Escande Award 1999 from the Toulouse Institut National Polytechnique–ENSEEIHT.

He is a member of the Sociedade Brasileira de Micro-ondas e Optoeletrônica (SBMO), Sociedade Brasileira de Eletromagnetismo (SBMag), Sociedade Brasileira de Microeletrôncia (SBMicro), and The applied Computacional Eletromagnetics Society (ACES). Since 2019, he has been an Associate Editor of the IEEE Latin America Transactions.

LALA RAJAOARISOA (Member, IEEE) received the M.Sc. degree and the Ph.D. degree in automatic and computer sciences from the University of Aix-Marseille, France, in 2005 and 2009, respectively. He is currently an Assistant Professor with the Institut Mines-Télécom Lille Douai. His research interests include the development of data-driven tools and methods for the observation and control of large-scale distributed systems. He develops predictive models and controllers to assess system behavior and optimize its performance. His development includes the analysis of intrinsic properties, such as stability, observability, identifiability, and controllability. He is involved in research activities dedicated to the optimization of energy efficiency of building systems and the control and management of hydraulic systems with more than 80 papers published in refereed journals and conferences. He regularly participates and contributes on several international projects (ANR, FUI, and INTERREG) and was the supervisor of more than of 15 Ph.D. students, postdocs, research engineers, and master's internships.

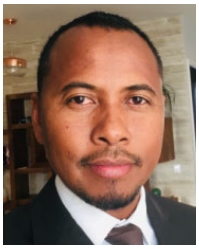

WENCESLAS RAHAJANDRAIBE (Member, IEEE) received the B.Sc. degree in electrical engineering from Nice Sophia-Antipolis University, France, in 1996, the M.Sc. degree (Hons.) in electrical engineering from the Science Department, University of Montpellier, France, in 1998, and the Ph.D. degree in microelectronics form the University of Montpellier. Since 1998, he has been with the Microelectronics Department of Informatics, Robotics and Microelectronics Laboratory of Montpellier (LIRMM). Since 2003, he joined the Microelectronic Department of Materials, Microelectronics and Nanoscience Laboratory of Provence (IM2NP), Marseille, France, where he was an Associate Professor. Since 2014, he has been a Professor with Aix-Marseille University, where he also heads the Integrated Circuit Design Group, IM2NP Laboratory. He is regularly involved to participate and to lead national and international research projects (ANR, H2020, and FP7 KIC-InnoEnergy). He directed and co-supervised 18 Ph.D. and 15 master students. His research interests include AMS and RF circuit design from transistor to architectural level. His present research activity is focused on ultralow power circuit design for smart sensor interface and embedded electronic in bioelectronic and e-health applications, wireless systems, design technique, and architecture for multi-standard transceiver. He is author or coauthor of 11 patents and more than 150 papers published in refereed journals and conferences. He is an expert for the ANR, the French Agency for Research. He has served on program committees of IEEE NEWCAS and ICECS. He has been and is a Reviewer of contributions submitted to several IEEE conferences and journals, such as ISACS, NEWCAS, MWSCAS, ESSCIRC, ESSDERC, RFIC, IEEE Transactions on Circuits and Systems I and II, and *IET Electronics Letters*.

RÉMY VAUCHÉ (Member, IEEE) received the M.Eng. degree in microelectronics and telecommunication from Polytech' Marseille, Marseille, France, in 2008, the M.S. degree in microelectronics and nanoelectronics from Aix-Marseille University, Marseille, in 2008, and the Ph.D. degree in microelectronics from the University of Provence, Marseille, in 2011.

From 2011 to 2014, he was a Lecturer and a Researcher with the ISEN French Engineering School, Toulon, France. Since 2014, he has been an Associate Professor with Aix-Marseille University. His current research interests include mainly the design of integrated circuits and systems for ultra-wideband impulse radio, human body communications, and home-care applications.

Dr.Dr. Vauché is a member of the Integrated Circuits Design Team, Provence Nanosciences Microelectronics, and Materials Laboratory, Marseille.

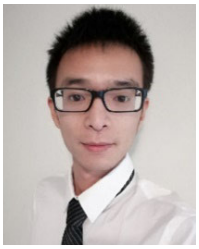

ZHIFEI XU (Member, IEEE) received the Ph.D. degree from the University of Rouen, France, in 2019. He is currently doing his Postdoctoral Research with the EMC-Laboratory, Missouri S&T, USA. His research interests include signal integrity, power integrity, and EMC analysis with different models on multilayer PCBs. He published book and extensive publications with related expertise in high-speed signal/power integrity and EMC design. He also developed Kron–Branin model for multilayer PCB modeling applications. His current publications are focusing on the advanced/optimized algorithms/tools with respect to the functions for signal/power and EMC analysis for high-speed PCB design.

FAYU WAN (Member, IEEE) received the Ph.D. degree in electronic engineering from the University of Rouen, Rouen, France, in 2011. From 2011 to 2013, he was a Postdoctoral Fellow with the Electromagnetic Compatibility Laboratory, Missouri University of Science and Technology, Rolla. He is currently a Full Professor with the Nanjing University of Information Science and Technology, Nanjing, China. His current research interests include negative group delay circuits, electrostatic discharge, electromagnetic compatibility, and advanced RF measurement.

JUNXIANG GE (Associate Member, IEEE) received the Ph.D. degree in radio engineering from Southeast University, Nanjing, China, in 1991. He has been the Dean of the School of Electronic and Information Engineering, Nanjing University of Information Science and Technology, Nanjing, since 2011. His current research interests include electromagnetic field theory, microwave and millimeter wave technology, and antenna.

SÉBASTIEN LALLÉCHÈRE (Member, IEEE) received the Ph.D. degree in electronics and electromagnetics from Université Blaise Pascal (UBP), Clermont-Ferrand, France, in 2006, and the French H.D.R. degree from Universté Clermont Auvergne (UCA), Clermont-Ferrand, in 2018. He served as Research Engineer with LASMEA, Clermont-Ferrand, France, in 2007, focusing on intensive computational methods for electromagnetics. He joined UBP, as an Assistant Professor in September 2007, and he has been an Associate Professor with UCA, since 2017, and with Institut Pascal, since 2012. His research interests include electromagnetic compatibility (EMC), antennas and propagation, complex systems, computational electromagnetics, reliability, stochastic, and sensitivity analysis for electrical engineering issues. He is actively involved in different research projects in antennas, RF, and EMC. Since 2019, he has been with the Head of the French URSI Commission E EM environment and interferences.